

Article

Functionalized Surface Layer on Poplar Wood Fabricated by Fire Retardant and Thermal Densification. Part 2: Dynamic Wettability and Bonding Strength

Demiao Chu ^{1,2}, Jun Mu ^{1,*}, Stavros Avramidis ³, Sohrab Rahimi ³, Shengquan Liu ² and Zongyuan Lai ¹

¹ Key Laboratory of Wood Material Science and Utilization (Beijing Forestry University), Ministry of Education, Beijing 100083, China; 13chudemiao@sina.cn (D.C.); lzy2015@bjfu.edu.cn (Z.L.)

² School of Forestry and Landscape Architecture, Anhui Agricultural University, Hefei 230036, China; liusq@ahau.edu.cn

³ Department of Wood Science, University of British Columbia, Vancouver, BC V6T 1Z4, Canada; stavros.avramidis@ubc.ca (S.A.); sohrab.rahimi@alumni.ubc.ca (S.R.)

* Correspondence: mujun@bjfu.edu.cn; Tel.: +86-010-62336053

Received: 9 October 2019; Accepted: 30 October 2019; Published: 5 November 2019



Abstract: In continuation of our former study on a novel combined treatment of nitrogen–phosphorus fire retardant and thermomechanical densification on wood, this study focuses on the dynamic wettability and the bonding strength. The contact angle was measured using the sessile drop method and the surface energy was calculated according to the van Oss method. Water surface penetrating and spreading is analyzed by both the Shi and Gardner model and the droplet volume changing model. The results reveal that the combined treatment increased the surface energy, especially the acid–base component. The contact angle declined and the water droplet spread more easily on the surface. Meanwhile, the rate of relative droplet volume decreased by 32.6% because the surface layer was densified and stabilized by the combined process. Additionally, the surface possesses the lowest roughness and highest abrasion resistance on the tangential section. Thus, the bonding strength of the combined treated poplar decreased by 29.7% compared to that of untreated poplar; however, it is still 53.3% higher than that of 220 °C heat-treated wood.

Keywords: combined treatment; wettability; surface free energy; bonding strength; poplar

1. Introduction

Wood is a renewable bioresource with many applications such as in construction, decoration, furniture, and cabinetry [1]. The demand for wood products in China has dramatically increased not only for esthetic reasons, but also because of government bonuses and mandates for using renewable materials mainly due to environmental concerns [2,3]. As a result, the demand for plantation trees has noticeably increased particularly due to forest product reduction. Nonetheless, the downside of using plantation timbers is substantially related to its low density, mechanical strength, and dimensional stability [4,5]. The service life of wood products depends on chemical or physical modifications. Density of wood is routinely considered to be one of the most important material characteristics on account of its strong correlation with strength [1,6]. Several thermomechanical (TM) methods have been developed for that purpose [7,8]. For further details, see Part 1 of our study [9].

Apart from the compression stability, the TM process may exacerbate the surface characteristics namely roughness and wettability, etc., which impacts bonding and coating performance [10–14].

Surface alteration is an indispensable part in the TM modification of wood; however, its wettability and bonding properties have not been well studied.

Nitrogen–phosphorus (NP) is an ecofriendly, benign, and affordable fire retardant [15]. Our research group attempted to enhance the leachability and hygroscopicity of NP, as well as smoke development during burning [16]. Recent studies revealed that NP also has an intensification effect on high-temperature (HT) treatment of wood [17,18]. In Part 1 of this study, it was reported that the combined process of using NP fire retardant and TM methods improved compression recovery and combustion safety. Since NP is a water-soluble chemical agent, it may enhance the hydrophilia of the treated wood. Here, we attempt to reveal the synergetic effects of this combined method on surface properties and bonding strength. The Shi and Gardner model and the droplet volume changing model are used to characterize the dynamic wetting process, and the surface characters and surface free energy are taken into account to explain bonding performance of the NP–HT combined treated wood.

2. Materials and Methods

2.1. Treatment

The NP–TM method was used to fabricate a certain thickness of functionalized surface layer on poplar (*Populus beijingensis* W. Y. Hsu). The treatment is the same as described in Part 1 [9].

2.2. Surface Free Energy

Surface free energy of wood is calculated mainly based on Young's equation. Two methods have been used for the calculation of the surface free energy, namely the van Oss-Chaudhury-Good (vOCG) theory. The Young equation is

$$\gamma_S = \gamma_L \cos\theta. \quad (1)$$

In the vOCG method, the surface free energy is expressed as

$$\gamma_S = \gamma_S^{LW} + \gamma_S^{AB} + 2(\gamma_S^- \gamma_S^+)^{1/2}. \quad (2)$$

Combining Equation (4) with Young's equation gives

$$\gamma_L (1 + \cos\theta) = 2(\gamma_S^{LW} \gamma_L^{LW})^{1/2} + 2(\gamma_S^+ \gamma_L^-)^{1/2} + 2(\gamma_S^- \gamma_S^+)^{1/2} \quad (3)$$

where γ_S and γ_L are the surface free energy of solids and liquid, respectively, γ_{SL} is the surface tension of the solid–liquid interface, and θ is the contact angle between a solid (*S*) and a liquid (*L*). The γ_{Sv} is the total surface energy calculated using the vOCG method, γ_S^{AB} is the acid–base based surface free energy for solids and liquid, γ_S^{LW} and γ_L^{LW} are, respectively, the Lifshitz–van der Waals-based surface free energy for solids and liquid, γ_S^+ and γ_S^- are, in turn, the acid-based surface free energy for solids and liquid, γ_S^- and γ_L^- are, respectively, the base-based surface free energy for solids and liquid. Distilled water, formamide, and diiodomethane, with known energy characteristics (Table 1), were used to calculate the surface free energy of treated wood samples [19].

Table 1. Surface tension and components of three different test liquids.

Liquids	Surface Free Energy (mJ m ⁻²)				
	γ_L	γ_L^{LW}	γ_L^{AB}	γ_L^+	γ_L^-
Distilled water	72.8	21.8	51.0	25.5	25.5
Diiodomethane	50.8	50.8	0	0	0
Formamide	58.0	39.0	19.0	2.28	39.6

2.3. Contact Angles and Dynamic Wettability

A surface contact angle instrument coupled with SCA 20 software (OCA 20 Data Physics Instruments GmbH, Filderstadt, Germany), wherein a video measuring system with a high-resolution CCD camera and a high-performance digitizing adapter that enables instantaneous recording of the image and calculation of the contact angle, was used. Every group contained five replicates (20 mm × 20 mm × thickness) and data were collected randomly from three sites on each sample, using an automatic microsyringe to dispense 1.5 µL drops of testing liquids on the surface.

Images of the droplet on the surface were taken and stored at intervals of 1 s during the first 10 s, then intervals of 5 s until the end of the test. The contact angle (θ), height (h) and liquid–wood interface diameter (d) of each droplet images were measured for further calculation. Thus, the wetting model of the water droplet volume changes (here named the D-V model) during the wetting process, could be calculated as

$$AR_t = 1 - (Vt/V_0) = a(1 - \exp(-K_a t)) \quad (4)$$

where AR_t is the absorption ratio at t (s), Vt and V_0 is the droplet volume at t (s) and 0 s, respectively; a is a material constant and K_a refers to the decrease rate of intrinsic relative droplet volume.

According to the Shi and Gardner (S-D model), the contact angle changes during the wetting process could be calculated as

$$\theta = (\theta_i \cdot \theta_e) / \{\theta_i + (\theta_e - \theta_i) \exp[K_\theta (\theta_e / (\theta_e - \theta_i)) t]\} \quad (5)$$

where θ is the contact angle at a certain time, θ_i and θ_e are the initial (instantaneous) and equilibrium contact angle, respectively; K_θ refers to how fast the liquid spreads and penetrates the porous structure of wood, which is a constant referred to the intrinsic decrease rate of relative contact angle. The t represents wetting time, then the θ_i , θ_e and K_θ values could be calculated. As the influence of water absorption, the wetting performance of the tested surface changes with time, and the instant decrease rate of contact angle (IK_θ) in the first 10 s was also calculated.

2.4. Surface Characteristics and Bonding Strength

Mass loss of surface abrasion for the processing layer was measured with a JM-IV instrument (Wuhan Gelaimo Testing Equipment Co., Ltd., Hubei, China), according to international standard ISO 7784-1 (1997). The wheel was coupled with 240-grit sanding paper during testing, and the mass loss values were calculated after 100 rotations. Surface roughness measurements were obtained by the stylus method in the perpendicular direction to the fibers on the wood surface and were carried out using a Taylor Hobson Surtronic 3+ instrument (Metrology Instrument Taylor Hobson Ltd., Leicester, England) at a constant speed of 1 mm/s over 15 mm of tracing length and a 2.5 mm cutoff across the sample grain. Bonding strength of treated wood was determined according to JAS234-2003 and STM D2559 using polyvinyl acetate glue (PVAc). After gluing (200 g m⁻²), the samples were pressed under 4 kg force (kgft) and maintained for 12 h.

3. Results and Discussion

3.1. Contact Angles and Surface Free Energy

Table 2 shows the contact angles of different test liquids. Calculation of the surface energies was conducted using contact angles of diiodomethane, distilled water, and formamide, wherein the diiodomethane was selected as nonpolar test liquid and the formamide was used as the polar test liquid. The contact angles of the formamide and diiodomethane were lower than that of water. For all samples investigated, the total surface free energy ranged from 39 to 57 mJ m⁻², which agrees with previous studies [20].

According to the vOCG theory, the total surface energy (γ_s) of the W_{NP-TM} was increased by the NP-HT treatment. The γ_s^{AB} value increased dramatically, while the γ_s^{LW} decreased by 7.6%.

The AB refers to acid–base interactions and is related to the hydrogen bond component and the LW is the London–van der Waals component. Both of the electron donors (γ_s^-) and acceptors (γ_s^+) were increased, wherein the γ_s^+ was proved less affected by the HT [20]. This result means that the treated poplar surface became more hydrophilic after the NP–HT, which helps water-based adhesives to spread and penetrate. The reason is that the nitrogen–phosphorus fire retardant used in the study is a water-soluble chemical, which could cause a small contact angle with distilled water [15,18]. The γ_s value of the W_{HT} samples decreased because of the HT, where the free reactive hydroxyl groups in hemicelluloses are partly removed [21,22]. The TM process further decreased the surface energy of the W_{HT-TM} samples. That result could be explained by the increased density and enhanced surface smoothness causing a lower contact area of liquid and wood fibrillation. Similarly, the surface smoothness and density enhancement in W_{TM} samples brought a considerable increase of the electron acceptor (γ_s^+) component of the surface energy.

Table 2. Contact angle and surface free energy of untreated and treated poplar.

Groups	Contact Angle (°)			Surface Free Energy (mJ m ⁻²)				
	Diiodomethane	H ₂ O	Formamide	γ_s	γ_s^{LW}	γ_s^{AB}	γ_s^+	γ_s^-
W_{NP-TM}	44.42 ± 2.42	64.98 ± 4.3	71.72 ± 2.68	55.13	37.32	17.81	2.15	36.9
W_{TM}	35.28 ± 4.73	115.24 ± 3.7	97.55 ± 5.28	45.80	41.90	3.90	6.76	0.56
W_{HT-TM}	41.21 ± 4.12	116.88 ± 8.7	73.28 ± 0.62	39.95	39.00	0.95	0.05	4.22
W_{HT}	38.56 ± 3.52	116.56 ± 6.8	69.99 ± 4.30	42.38	40.32	2.06	0.20	5.42
W_c	38.40 ± 1.14	71.58 ± 1.6	59.30 ± 0.83	45.65	40.41	2.18	0.08	15.12

3.2. Dynamic Wetting Process

Representative images of water droplets and contact angle curves of untreated and treated samples are illustrated in Figure 1. It can be seen that all contact angles are decreasing as a function of testing duration.

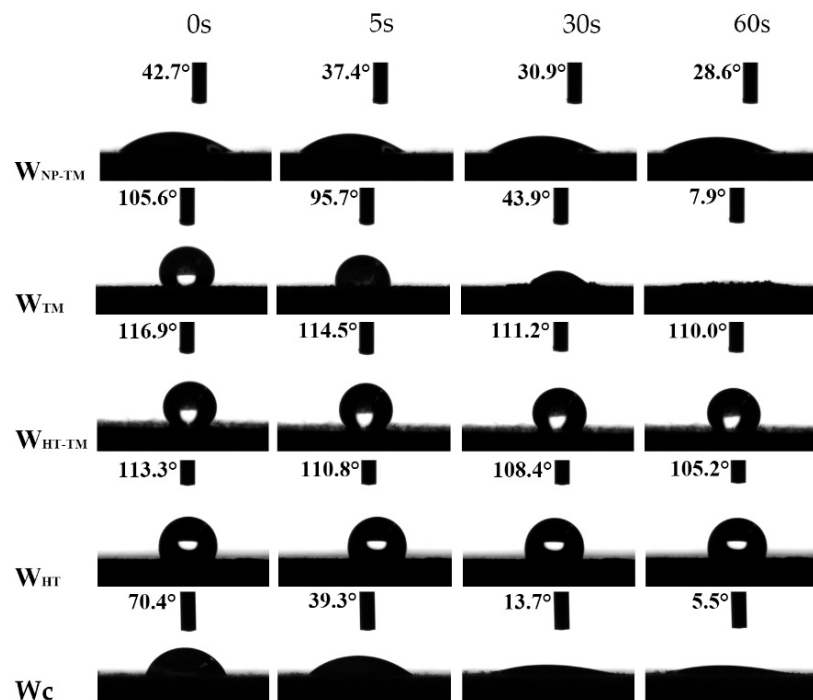


Figure 1. Images of water droplets on surface of untreated and treated poplar.

As seen in Figure 1, the untreated poplar possessed a low contact angle of 70.4° at 0 s, and the volume of the water droplet decreased quickly within 60 s. After 220 °C HT for 2 h, the contact angle

of W_{HT} became much higher than that of W_c . The contact angle of W_{HT-TM} was further enhanced because of the TM process. Similarly, the contact angle at 0 s on the W_{TM} was around 50% higher than that of W_c , whereas it decreased sharply as the test time proceeded. It can be clearly observed that the surface swelled from the image at 30 s. In addition, the contact angle was 7.9° and the droplet almost disappeared at 60 s. For the W_{NP-TM} , the contact angle at 0 s was even lower than that of W_c , while it maintained a relatively stable value after 5 s. The contact angle reduced around 33% after 60 s, which was much lower than that of W_{TM} and W_c . Moreover, there was no swelling observed even at the interface of water droplet and wood surface. This could be explained by the high water solubility of the NP fire retardant. Contrary to that of W_{TM} , the contact angle of W_{NP-TM} was much more stable during the whole wetting process, and the enhanced compression stability of the surface relieved the decline of contact angle.

During the wetting process, the decline of the contact angle on the wood surface is caused by both spreading and penetration of the water droplets. The differences existed on both the initial contact angle and the decline rate during the test. Figure 2 illustrates the fitting curves of contact angle, instant decrease rate of contact angle IK_θ value, and the absorption ratio of untreated and treated poplar.

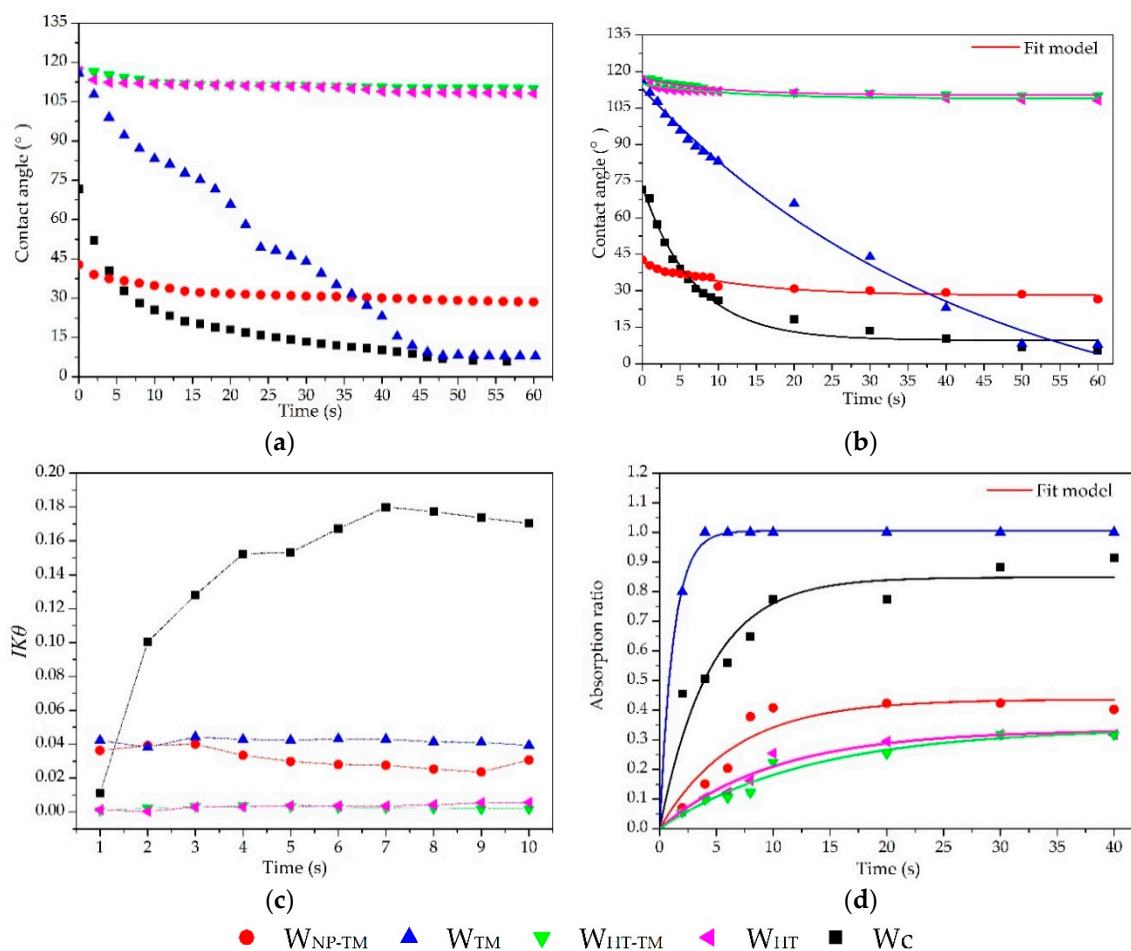


Figure 2. Contact angle curves (a), fitting curves of contact angle (b), instant decrease rate of contact angle IK_θ (c), and absorption ratio of the water droplet (d) on the surface of untreated and treated poplar.

The calculation of contact angle and absorption ratio changes was done according to the contact angle changing model (S-D wetting model) and droplet volume changing model (D-V wetting model), respectively, in order to further prove the hypothesis (Table 3). The R^2 values of the wetting models are higher than 0.95 for most samples.

Table 3. Wetting kinetics of water droplets on untreated and combined treated poplar.

Groups	Contact Angle Change				Absorption Ratio Change		
	θ_i (Degrees)	θ_e (Degrees)	K_θ	R^2	K_a	R^2	SE
W_{NP-TM}	41.92	26.24	0.019	0.90	0.153	0.907	0.034
W_{TM}	115.94	0.1 *	0.040	0.99	0.826	0.998	0.036
W_{HT-TM}	116.36	109.60	0.004	0.95	0.076	0.959	0.013
W_{HT}	113.79	105.98	0.002	0.96	0.099	0.966	0.014
Wc	68.73	3.42	0.174	0.92	0.227	0.928	0.039

Note: * means that we presumed the θ_e value of W_{TM} to be 0.1.

In the S-D model, the K_θ value reflected the shape of the wetting curve. The K_θ value of the W_{HT-TM} was 97.70% lower than Wc. The reduction of the K_θ value revealed the decline of the water spread and penetration on the surface. The initial (θ_i) and equilibrium (θ_e) contact angles of Wc was 68.73° and 3.42°, respectively. Due to HT, the θ_i value of W_{HT} increased by 65.56%. Besides, the decrease between θ_i and θ_e was only 6.86%, which indicated that the water droplet changed slightly during the wetting process. For the post-TM-treated samples of W_{HT-TM} , the K_θ values increased. This result could be caused by the enhancement of surface smoothness, thus making the water droplet more easily spread on the surface.

As illustrated in Figure 2a, the curve of contact angle for W_{TM} showed two broad peaks between 10 s to 40 s, the contact angle of W_{TM} declined until the end of the test. The θ_e value was almost zero, here we presumed it to be 0.1. The contact angle of W_{HT} only had a mild decline within the first 10 s and thereafter kept a relatively stable value. There is no obvious difference in the contact angle curve between W_{HT-TM} and W_{HT} , revealing that the post-TM process could not make it more hydrophobic. The increased density could be the reason for the increase of θ_i on the W_{TM} , while the low compression stability caused the decline of the contact angle.

According to Figure 2b, the fitting curves of W_{TM} and Wc decreased sharply at the beginning stage. For the W_{TM} , the contact angle declined until the end of the test. The surface swelling probably alleviated the decrease of the contact angle, causing an inclination to a linear function than the reality. The wettability of the testing surfaces changed as the wetting time increased.

It is worth noting that the θ_i on the W_{NP-TM} decreased significantly, that is 39.15% lower than that of Wc. Nevertheless the contact angle decrease trend and fitting curve assembled with that of W_{HT} and W_{HT-TM} (Figure 2a,b). Besides, the θ_e value was much higher than that of W_{TM} and Wc, revealing that the volume of the water droplet changed less. The instant decrease rate of contact angle value (IK_θ) of Wc increased, while the IK_θ values of W_{NP-TM} , W_{HT-TM} , and W_{HT} were stable, indicating that the water droplets had a weak effect on the surface at the beginning stage (Figure 2c). The alleviation effect on the decrease of the contact angle could also make the IK_θ value of W_{TM} more stable and lower than the reality. The θ_i value of W_{NP-TM} was the lowest because the NP fire retardant used in this study has a high hygroscopicity [15]. The lower decline could be explained by the increased surface density and high compression stability, as stated in Part 1.

In the D-V model, the K_a value reflects the change of absorption ratio; a smaller K_a value reveals a lower decrease rate of the droplet volume. The K_a of the water droplet on all the testing surfaces increased sharply at first, then reached a constant value as the time increased (Figure 2d). The only TM samples of W_{TM} has the highest K_a value, additionally, the absorption ratio curve reached the maximum within 5 s. It could be concluded that the water droplet on W_{TM} was mostly absorbed in the beginning stage. In favor of the result of S-D wetting model, the absorption ratio curve of W_{NP-TM} resembled with that of W_{HT-TM} and W_{HT} . This means that the W_{NP-TM} , W_{HT-TM} , and W_{HT} possessed favorable resistance to water. In other words, the water droplet infiltrated less into the surface layer.

3.3. Surface Characteristics and Bonding Strength

The TM process also exacerbates the surface characteristics and affects the bonding or coating performance [13,14]. Surface roughness, abrasion resistance, and bonding strength of all the treated samples are lower than that of untreated poplar, as illustrated in Figure 3.

As shown in Figure 3a, the TM process significantly enhanced the surface smoothness of W_{HT-TM} , W_{TM} , and W_{HT-TM} ; this is because the surface roughness was flattened in these samples. Among those compressed samples, the W_{NP-TM} has the lowest roughness values, including the mean arithmetic deviation of the profile (Ra), root-mean-square roughness (Rq), and mean peak-to-valley height (Rz). The filling effect of the NP probably further enhanced the surface roughness. Besides, HT also enhanced the surface roughness for W_{HT} , which agrees with other studies [23].

Compared to the W_c , the abrasion mass loss of W_{HT} increased sharply (Figure 3b). The abrasion performance related to the shearing strength of the surface; the TM treatment enhanced the surface density mainly by reducing the pore and lumen structures. The degradation of the cell wall chemical components made the surface more brittle; thus, the enhancement of W_{HT-TM} was limited. Additionally, the cracks in cell walls due to the TM may further decrease the abrasion resistance; the mass loss of W_{TM} was higher than that of W_c , although the surface density increased. Since the cell walls were mostly undamaged and the NP recrystallized in the pores, the abrasion resistance of the W_{NP-TM} remained at the same level as the W_c . The slight decrease of abrasion could be explained by the decomposition and catalytic dehydration effects of the NP on the cell wall under hot press conditions [17].

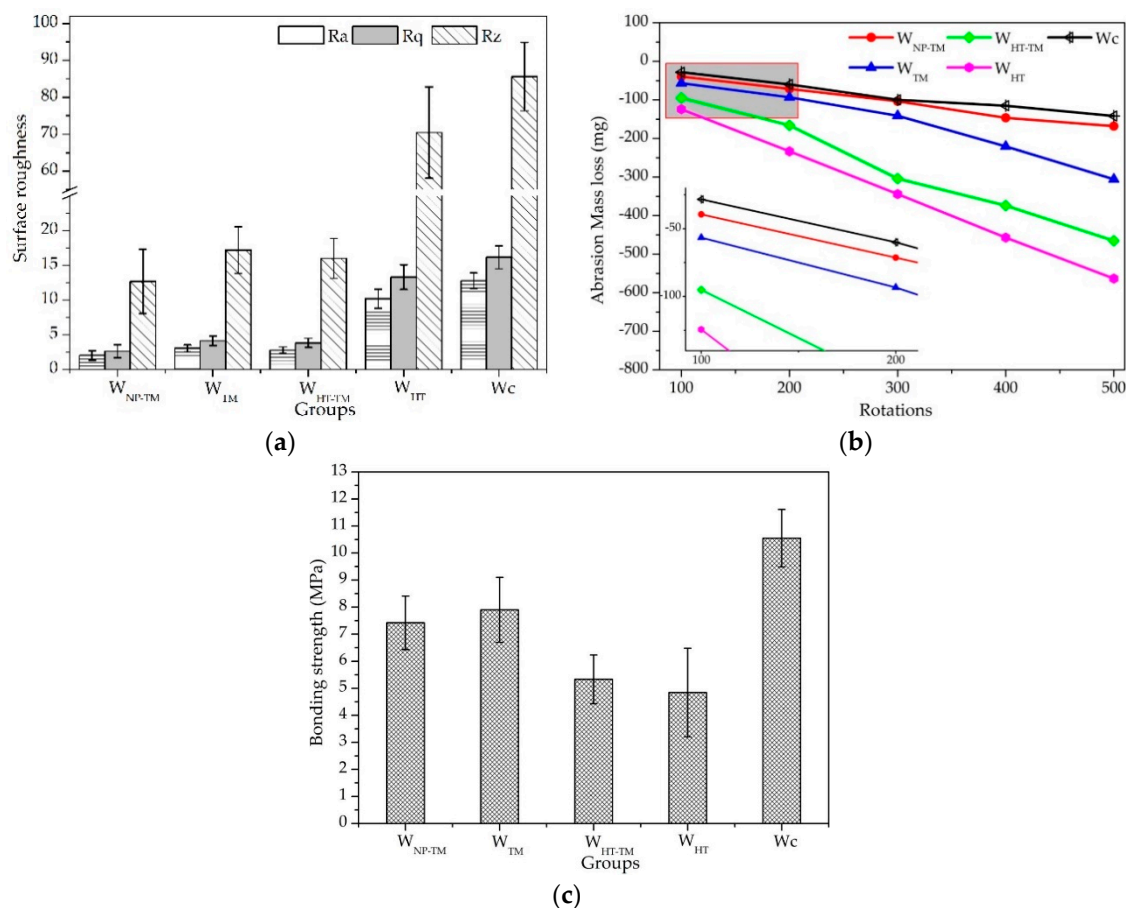


Figure 3. The surface roughness (a), abrasion mass loss (b), and bonding strength (c) of untreated and treated poplar.

As shown in Figure 3c, the bonding strength of all treated poplar decreased, especially the W_{HT} samples. The bonding strength of the W_{HT-TM} increased slightly as the surface hardness and abrasion

resistance increased by the TM process, although the wetting properties were not enhanced. For the NP–TM treated poplar, the bonding strength of W_{NP-TM} was 29.67% lower than that of W_c , which could be explained by the low permeability, as discussed according to D-V model. The adhesive hardly goes into the gaps and fewer interactions existed between the wood and adhesive. Conversely, the wetting process was so fast that too much adhesive absorbed into the surface layer and the glue line was weak for W_{TM} .

4. Conclusions

This work further investigated the effect of nitrogen–phosphorus fire retardant (NP) pre-impregnation and the thermomechanical densification (TM) process on poplar wood. This NP–TM combined treatment could increase the surface energy and improve the spreadability of water on wood surfaces, which enhances the contact effect between wood and adhesive. However, the surface layers of the NP–TM combined treated poplar were highly condensed and stabilized, which prevents the permeation of the liquid on the surface. In addition, the NP–TM-treated wood possessed the lowest roughness and highest abrasion resistance on the functionalized surface. Therefore, it conversely influences the interactions of adhesive and pores on the surface. The low compression stability of the TM-only treated poplar causes surface swelling during the wetting process and decreases the bonding strength. Compared with that of wood that was only heat-treated, the surface bonding strength of the NP–TM combined treated poplar increased by 53.3%. In future studies, it is worth investigating possible methods for enhancing wetting performance and bonding strength while keeping the compression stability of this functionalized surface layer, making this new material more useful for the wood industry.

Author Contributions: Conceptualization, D.C. and J.M.; Methodology, D.C. and J.M.; Software, D.C. and S.R.; Validation, J.M., S.A., and S.L.; Formal Analysis, D.C., J.M., and Z.L.; Investigation, D.C. and J.M.; Resources, D.C. and J.M.; Data Curation, D.C., S.R., and J.M.; Writing–Original Draft Preparation, D.C.; Writing–Review & Editing, J.M., S.A., S.L., S.R., and Z.L.; Visualization, D.C.; Supervision, J.M. and S.A.; Project Administration, J.M.; Funding Acquisition, J.M.

Funding: This research was funded by the Forestry Public Welfare Project Foundation of China, grant number 201404502, and the Fundamental Research Funds for the Central Universities of China, grant number 2015ZCQ-CL-01.

Conflicts of Interest: The authors declare no conflict of interest.

References

- Hill, C.A.S. *Wood Modification: Chemical, Thermal and Other Processes*; John Wiley & Sons: Chichester, UK, 2006.
- Lin, H.; Wang, Y.; Chen, Z.D.; Yang, B.X. Progress & Application Prospects of Modified Wood. *For. Mach. Woodwork. Equip.* **2006**, *34*, 11–13.
- Yuan, Q.P.; Su, C.W.; Xiong, J.B. Research Progress of Plantation Wood Machining Properties. *J. Anhui Agric. Sci.* **2011**, *3*, 42–45.
- Kiaei, M.; Naji, H.R.; Abdul-Hamid, H.; Farsi, M. Radial variation of fiber dimensions, annual ring width, and wood density from natural and plantation trees of alder (*Alnus glutinosa*) wood. *Drev. Vysk. Wood Res.* **2016**, *61*, 55–64.
- Xu, K.; Lu, J.X.; Li, X.J.; Wu, Y.Q. Effect of heat treatment on dimensional stability of phenolic resin impregnated poplar wood. *J. Beijing For. Univ.* **2015**, *37*, 70–77.
- Fang, C.H.; Mariotti, N.; Cloutier, A.; Koubaa, A.; Blanchet, P. Densification of wood veneers by compression combined with heat and steam. *Eur. J. Wood Prod.* **2012**, *70*, 155–163. [[CrossRef](#)]
- Laskowska, A. The Influence of Process Parameters on the Density Profile and Hardness of Surface-densified Birch Wood (*Betula pendula* Roth). *BioResources* **2017**, *12*, 6011–6023. [[CrossRef](#)]
- Kariz, M.; Kuzman, M.K.; Sernek, M.; Hughes, M.; Rautkari, L.; Kamke, F.A.; Kutnar, A. Influence of temperature of thermal treatment on surface densification of spruce. *Eur. J. Wood Prod.* **2017**, *75*, 113–123. [[CrossRef](#)]

9. Chu, D.M.; Mu, J.; Avramidis, S.; Rahimi, S.; Liu, S.Q.; Lai, Z.Y. Functionalized surface layer on poplar wood fabricated by fire retardant and thermal densification. Part 1: Compression recovery and flammability. *Forests* **2019**, *10*, 955. [[CrossRef](#)]
10. Bekhta, P.; Proszkyk, S.A.; Krystofiak, T. Colour in short-term thermo-mechanically densified veneer of various wood species. *Eur. J. Wood Prod.* **2014**, *72*, 785–797. [[CrossRef](#)]
11. Darwis, A.; Wahyudi, I.; Dwianto, W.; Cahyono, T.D. Densified wood anatomical structure and the effect of heat treatment on the recovery of set. *J. Indian Acad. Wood Sci.* **2017**, 1–8. [[CrossRef](#)]
12. Chen, A.T.; Luo, P.P.; Xu, Z.Y.; Hu, Z.J. Effects of silicon dioxide combined heat treatment on properties of rubber wood. *J. For. Eng.* **2016**, *1*, 21–25. (In Chinese) [[CrossRef](#)]
13. Liu, H.L.; Shang, J.; Kamke, F.A.; Guo, K.Q. Bonding performance and mechanism of thermal-hydro-mechanical modified veneer. *Wood Sci. Technol.* **2018**, *52*, 343–363. [[CrossRef](#)]
14. Pelit, H.; Budakçı, M.; Sönmez, A.; Burdurlu, E. Surface roughness and brightness of scots pine (*Pinus sylvestris*) applied with water-based varnish after densification and heat treatment. *J. Wood Sci.* **2015**, *61*, 586–594. [[CrossRef](#)]
15. Gu, B. Study on the Effects of Properties of UF Plywood Treated with BL-Environmental-Friendly Flame Retardant. Composition Analysis of BL Environmental Protection Flame Retardant. Ph.D. Thesis, Beijing Forestry University, Beijing, China, 2007; pp. 50–56.
16. Zhang, X.T.; Mu, J.; Chu, D.M.; Zhao, Y. Synthesis of fire retardants based on N and P and poly (sodium silicate aluminum dihydrogen phosphate) (PSADP) and testing the flame-retardant properties of PSADP impregnated poplar wood. *Holzforschung* **2015**, *70*, 341–350. [[CrossRef](#)]
17. Chu, D.M.; Mu, J.; Zhang, L.; Li, Y.S. Promotion effect of NP fire retardant pre-treatment on heat-treated poplar wood. Part 1: Color generation, dimensional stability, and fire retardancy. *Holzforschung* **2017**, *71*, 207–215. [[CrossRef](#)]
18. Chu, D.M.; Mu, J.; Zhang, L.; Li, Y.S. Promotion effect of NP fire retardant pre-treatment on heat-treated poplar wood. Part 2: Hygroscopicity, leaching resistance, and thermal stability. *Holzforschung* **2017**, *71*, 217–223. [[CrossRef](#)]
19. Van Oss, C.J.; Good, R.J.; Chaudhury, M.K. Additive and nonadditive surface tension components and the interpretation of contact angles. *Langmuir* **1988**, *4*, 884–891. [[CrossRef](#)]
20. Gérardin, P.; Petrič, M.; Petrissans, M.; Lambert, J.; Ehrhardt, J.J. Evolution of wood surface free energy after heat treatment. *Polym. Degrad. Stab.* **2007**, *92*, 653–657. [[CrossRef](#)]
21. Wang, W.; Zhu, Y.; Cao, J.Z.; Sun, W.J. Correlation between dynamic wetting behavior and chemical components of thermally modified wood. *Appl. Surf. Sci.* **2015**, *324*, 332–338. [[CrossRef](#)]
22. Gao, X.; Zhou, F.; Fu, Z.Y.; Zhou, Y.D. Sorption isotherms characteristics of high temperature heat-treated *Picea abies* and *Pseudotsuga menziesii*. *J. For. Eng.* **2018**, *3*, 25–29. [[CrossRef](#)]
23. Salca, E.; Hiziroglu, S. Evaluation of hardness and surface quality of different wood species as function of heat treatment. *Mater. Des.* **2014**, *62*, 416–423. [[CrossRef](#)]

